BNL-225313-2024-JAAM

Role of Heterointerface in Lithium-Induced Phase Transition in Td-WTe2 Nanoflakes

S. Xu, K. Evans-Lutterodt

To be published in "ACS Applied Electronic Materials"

February 2024

Photon Sciences

Brookhaven National Laboratory

U.S. Department of Energy

USDOE Office of Science (SC), Basic Energy Sciences (BES). Scientific User Facilities (SUF)

DISCLAIMER

Role of Heterointerface in Lithium-Induced Phase Transition in T_d-WTe_2 Nanoflakes

*Shiyu Xu1,2‡, Mengjing Wang1‡, Maria Bambrick-Santoyo3, Kenneth Evans-Lutterodt4, Natalie L. Williams1,5, Judy J. Cha1**

1 Department of Materials Science and Engineering, Cornell University, Ithaca, NY 14853, USA.

2 Department of Mechanical Engineering and Materials Science, Yale University, New Haven, CT 06511, USA.

3 Department of Applied Physics, Yale University, New Haven, CT 06511, USA.

4 National Synchrotron Light Source II, Brookhaven National Laboratory, Upton, NY 11973, USA.

5 Department of Chemistry and Chemical Biology, Cornell University, Ithaca, NY 14853, USA.

*Correspondence to: jc476@cornell.edu

‡ Co-first author

KEYWORDS

Lithium intercalation, phase transition, interface, WTe_2-hBN interface, *in-situ* Raman spectroscopy

ABSTRACT

A new polytype of WTe_2 with a bandgap has been recently discovered through the intercalation of lithium into the van der Waals gaps of T_d-WTe_2. Here, we report the effects of reduced thicknesses and heterointerfaces on the intercalation-induced phase transition in WTe_2. Using *in-situ* Raman spectroscopy during the electrochemical lithiation of WTe_2 flakes as a function of flake thickness, we observe a phase transition delay from T_d-WTe_2 to the new lithiated T_d' phase in 7- and 5-layered samples. We ascribe this suppression of the phase transition to the interfacial interaction between the nanoflake and the SiO_2/Si substrate, which plays an increasing role as the sample thickness is reduced. The suppressed kinetics of the phase transition can be mitigated by placing the WTe_2 flake on a hexagonal boron nitride (hBN) flake, which facilitates the release of the in-plane strain induced by the phase transition. Our study underscores the significance of interfacial effects in modulating phase transitions in two-dimensional (2D) materials, suggesting heterogeneous transition pathways as well as interfacial engineering to control these phase transitions.

INTRODUCTION

Two-dimensional (2D) transition metal dichalcogenides (TMDCs) have been extensively studied for their potential in various cutting-edge applications such as optoelectronics, electronics, catalysis, and energy storage, owing to their numerous structural polymorphs.[1-5] Phase transitions

in 2D TMDCs can be realized through methods including charge doping,[6] strain engineering,[7] intercalation,[8-9] thermal treatment,[10] and light irradiation.[11] Phase transitions in monolayer or few-layered TMDCs are highly desirable to minimize power consumption and realize ultimate scalability in many applications.[12-13] However, reduced thickness and the presence of heterointerfaces can significantly alter the phase transition thermodynamics and kinetics,[14-16] requiring a detailed understanding of the effects of thickness confinement and heterointerfaces for successful applications of 2D materials. Among 2D TMDCs, orthorhombic tungsten ditelluride (T_d-WTe_2) stands out as a type-II Weyl semimetal in bulk, and in the monolayer limit, a topological insulating phase,[17] superconductivity,[18-20] and ferroelectricity[21] have been observed. A new polytype of T_d-WTe_2, driven by lithiation, was recently discovered, exhibiting a unique crystal structure (T_d')[22] with a bandgap opening of 0.14 eV.[23] This discovery makes T_d-WTe_2 promising for applications in strained actuators and resistive memory. Yet, this phase transition was only observed in T_d-WTe_2 nanoflakes thicker than 30 nm, and effects of reduced thickness and heterointerfaces have not been explored.

In this study, we investigate the impact of thickness and heterointerfaces on the phase transition from the semi-metallic T_d-WTe_2 phase to the new lithiated T_d'-WTe_2 phase. This transformation was achieved by electrochemically inserting lithium into the van der Waals (vdW) gaps of the T_d-WTe_2 flake. For T_d-WTe_2 flakes with thicknesses raging from 30 to 100 nm (> 40 layers), the phase transition occurred at an applied electrochemical intercalation voltage of 0.8 V, as evident from the emergence of a distinct Raman spectrum and a lattice expansion in the out-of-plane direction. By contrast, for 7- and 5-layered T_d-WTe_2 flakes, the electrochemical intercalation voltage required for the phase transition was lowered to 0.5 V, indicating a suppression of phase transition energetics. We attribute this suppression to the strong interfacial interaction between the

T_d-WTe_2 flake and the SiO_2/Si substrate. This interfacial effect becomes more pronounced for thinner flakes and hinders the release of the in-plane strain introduced during the phase transition. Heterointerface engineering, whereby a WTe_2 – hBN interface was introduced to help facilitate the in-plane strain release, can mitigate the phase transition delay for thin WTe_2 flakes. Our observations underscore the significant influence of thickness and substrate heterointerfaces on phase transition dynamics of 2D materials.

RESULTS AND DISCUSSION

Electrochemical Intercalation in Thick T_d-WTe_2 Nanoflakes

Electrochemical intercalation cells that incorporate nanodevices were used to understand the phase transition of T_d-WTe_2 flakes induced by lithium intercalation.[24] These cells enable *in-situ* Raman spectroscopy or single-crystal X-ray diffraction (XRD) measurements as a function of intercalation (Figure 1a, Experimental Methods). The mechanically exfoliated T_d-WTe_2 flakes were 20 to 50 μm in lateral dimensions and 30 to 100 nm (> 40 layers) in thickness. Both liquid and polymer-based electrolytes were used for lithium intercalation (details in Experimental Methods).[25] By applying a controlled electrochemical intercalation voltage (V_{EC}) between the single crystalline T_d-WTe_2 flake (cathode) and the lithium (Li, anode), lithium ions (Li^+) are controllably driven and inserted into the vdW gaps of the T_d-WTe_2 flake. The applied V_{EC} lies between the open-circuit voltage (OCV, typically 2.3 - 2.8 V vs. Li^+/Li) and 0.1 V (vs. Li^+/Li). A lower V_{EC} corresponds to higher lithium concentrations in the T_d-WTe_2 flake, allowing for the fine-tuning of intercalation concentrations.

As reported previously by Muscher et al.[22] and Wang et al.[23], we observe a new polytype in WTe_2 flakes by intercalating lithium, which was confirmed by distinct Raman peaks that emerge

at V_{EC} of 0.8 V vs. Li^+/Li for a polymer cell (Figure 1c) and of 1.2 V vs. Li^+/Li for a liquid cell (Figure S1, Supporting Information). Raman peaks corresponding to T_d-WTe_2 at ~80.8, ~113, ~133, ~165 and ~212 cm^{-1} displayed noticeable shifts, broadening, or weakening, while several small new peaks emerged. The Raman spectrum of this new phase is that of lithiated T_d'-WTe_2.[22-23] Optical images show dark streaks in the lithiated T_d'-WTe_2 along the crystallographic axis b, which is perpendicular to the W-W chain of pristine T_d-WTe_2 (Figure 1b). These streaks were identified as wrinkles in the flake, as confirmed by scanning electron microscopy (SEM) on a post-intercalation cell (Figure S1). The formation of wrinkles is a result of the anisotropic in-plane strain introduced during the T_d to T_d' phase transition.

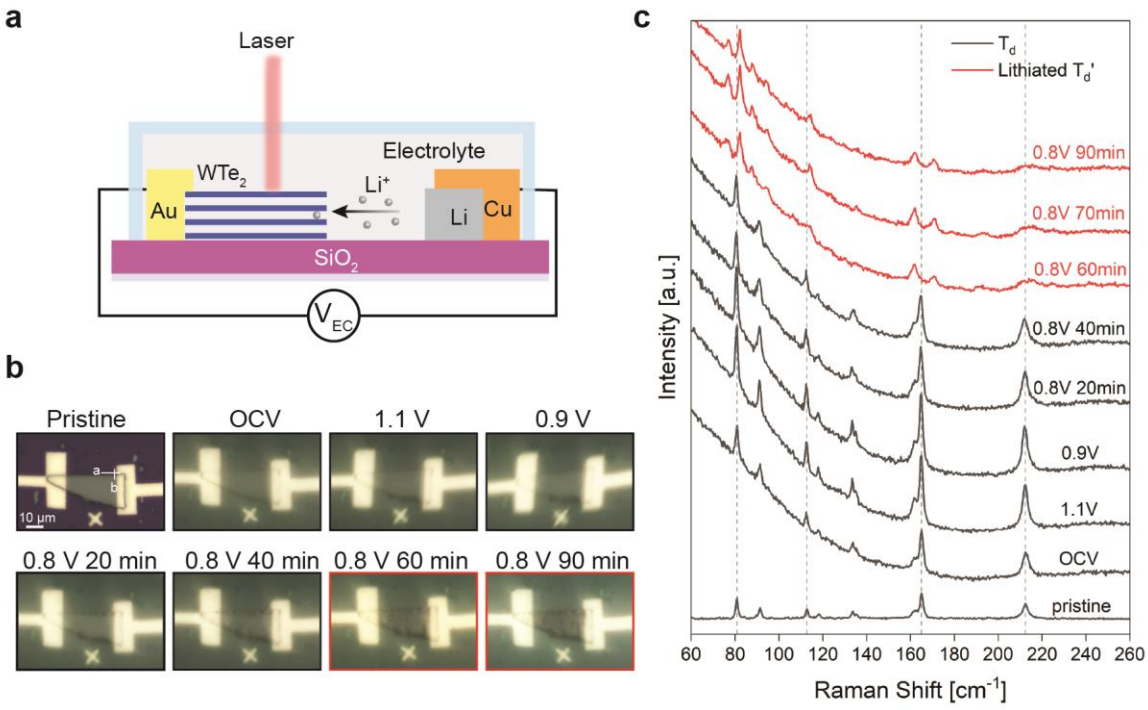

Figure 1. Lithium-induced phase transition in a thick T_d-WTe_2 nanoflake. (a) Schematic of a planar electrochemical intercalation cell with *in-situ* Raman capability. V_{EC} stands for the electrochemical intercalation voltage applied between the single crystalline T_d-WTe_2 nanoflake

and the lithium electrode. (b) Optical images of a thick T_d-WTe_2 nanoflake as a function of V_{EC} using a polymer electrolyte; scale bar, 10 μm. The black and red frames represent the T_d and lithiated T_d' phases, respectively. The T_d to T_d' phase transition is accompanied with the emergence of optically dark streaks across the nanoflake. (c) *In-situ* Raman spectra of the T_d-WTe_2 nanoflake in (b) as a function of intercalation voltage. The black and red spectra represent the T_d and lithiated T_d' phases, respectively.

Lattice Expansion of Lithiated T_d'-WTe_2 Nanoflakes

In addition to the in-plane strain, an out-of-plane expansion was observed through the change in the reciprocal lattice of the (002) plane, as determined by *in-situ* single-crystal XRD during electrochemical lithiation on individual flakes. Figure 2a illustrates the reciprocal lattice of the (002) plane for pristine T_d-WTe_2 (top), lithiated T_d'-WTe_2 (middle) and de-lithiated T_d-WTe_2 (bottom). In comparison to the pristine T_d-WTe_2, lithiated T_d'-WTe_2 shows a smaller lattice of the (002) plane in reciprocal space, which corresponds to an expansion in the out-of-plane c direction in real space. The c lattice of lithiated T_d'-WTe_2 was measured to be 14.82 Å, while that of the pristine T_d-WTe_2 was 14.05 Å (Figure 2c), representing a ~5.5% expansion of c lattice (Figure 2b). Notably, the co-presence of the intense peak of lithiated T_d'-WTe_2 and the weaker peak of T_d-WTe_2 indicates an incomplete phase transition of the T_d-WTe_2 nanoflake, which is a common occurrence in very thick flakes. After the acquisition of single-crystal XRD for the lithiated T_d'-WTe_2, the applied V_{EC} was removed, allowing for the nanoflake to recover to its original T_d phase. This recovery was confirmed by the disappearance of the lithiated T_d'-WTe_2 peak and restoration of a high intensity of the T_d-WTe_2 peak. This result demonstrates the reversibility of the T_d and T_d' phase transition.

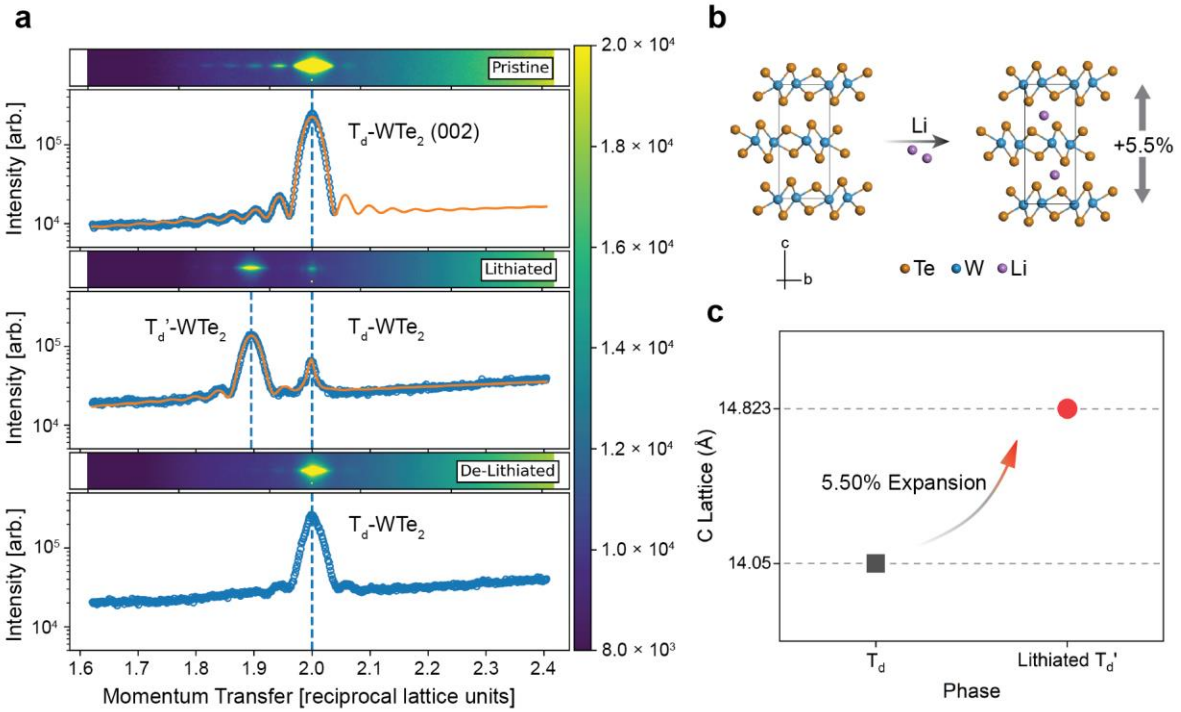

Figure 2. Lattice expansion of a thick T_d-WTe_2 nanoflake induced by lithium intercalation. (a) Diffraction spots and their corresponding intensity profiles of the (002) plane in the reciprocal space by single-crystal XRD collected from a thick T_d-WTe_2 nanoflake at the pristine T_d (top), lithiated T_d' (middle) and de-lithiated T_d (bottom) phases, respectively. (b) Side view of the structure change in the c direction of T_d-WTe_2 induced by lithium intercalation. Te: gold, W: blue, Li: purple. (c) Lattice expansion in c direction between the T_d and lithiated T_d' phases derived from single-crystal XRD.

Delayed Phase Transition in Few-layered T_d-WTe_2 Nanoflakes

Next, we performed lithium intercalation in thinner T_d-WTe_2 nanoflakes. While thicker T_d-WTe_2 flakes underwent the phase transition from T_d to the lithiated T_d' phase at an applied V_{EC} of 0.8 V

(vs. Li^+/Li), the same phase transition did not occur until 0.5 V (vs. Li^+/Li) for a 7-layered T_d-WTe_2 flake, as shown in Figure 3a. Optical images showed no obvious dark streaks after the T_d to T_d' phase transition; but, small wrinkles were observed with SEM post intercalation (Figure S2). For a 5-layered T_d-WTe_2 flake, *in-situ* Raman peaks persisted even at 0.4 V for over 40 minutes before eventually changing at 0.3 V (Figure 3b). Thus, our key finding is that thin T_d-WTe_2 flakes require more applied V_{EC} to induce the phase transition from T_d to the lithiated T_d' phase, indicating a suppression of the phase transition.

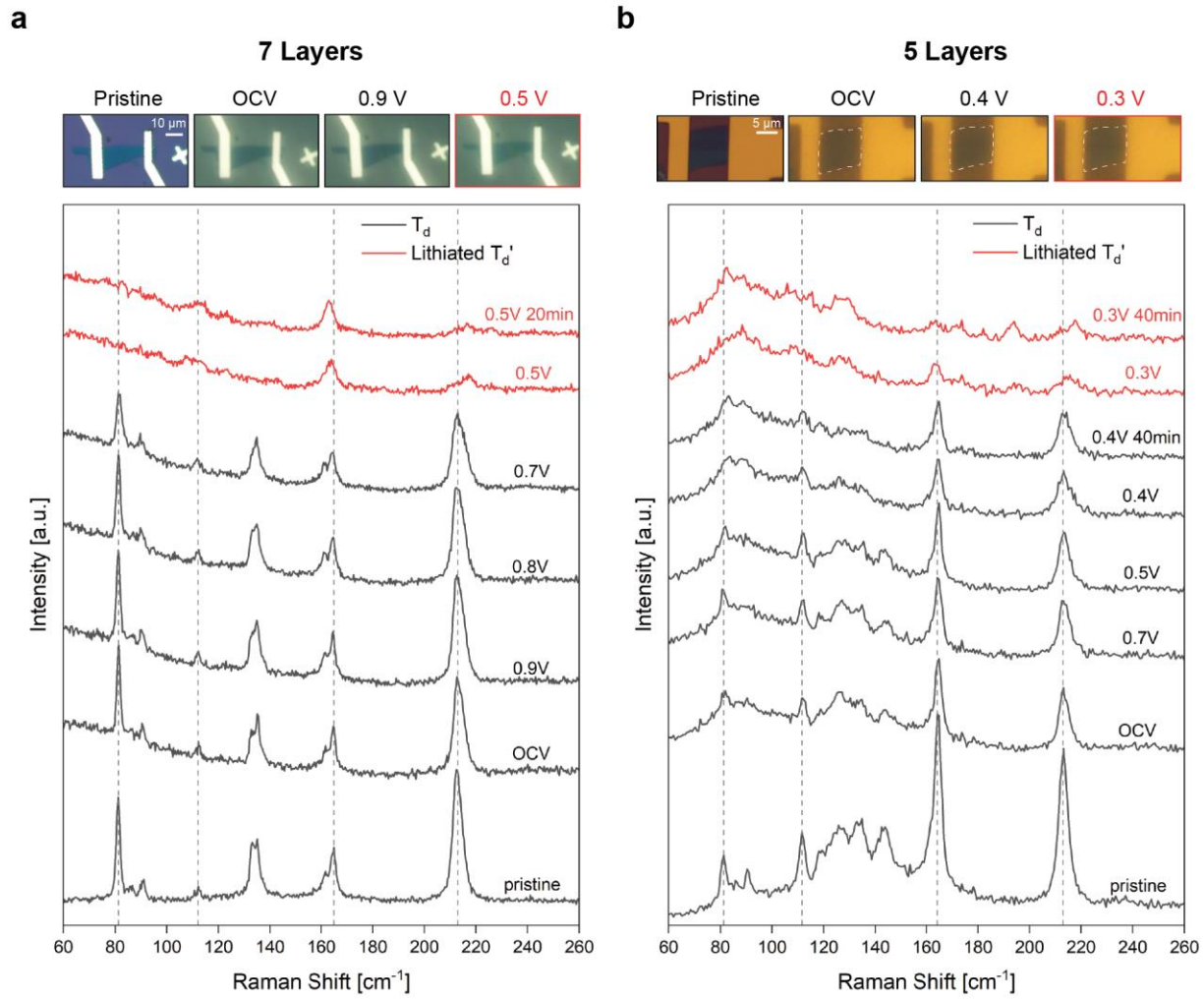

Figure 3. Delayed T_d to lithiated T_d' phase transition observed in few-layered samples. (a, b) Optical images (top) and *in-situ* Raman spectra (bottom) of a 7-layered (a) and a 5-layered (b) T_d-WTe_2 nanoflake during lithium intercalation; scale bar, 10 μm in (a) and 5 μm in (b). Black and red spectra represent the T_d and lithiated T_d' phases, respectively.

We consider several possibilities that can explain the suppression of the phase transition for thinner flakes: thickness-dependent band structure of T_d-WTe_2, suppressed nucleation of a T_d' phase with decreasing thickness, thickness-dependent bending-induced strain introduced by the out-of-plane expansion, and substrate interactions. These possibilities are discussed in order. First, if the band structure of T_d-WTe_2 changes with thickness, this might influence the intercalation-induced phase change as the process of lithium intercalation is to align the Fermi level between lithium and WTe_2. We rule this out because the semi-metallic nature of T_d-WTe_2 remains mostly unchanged with decreasing thickness.[26] The second possibility involves the suppression of nucleation of the new phase in thin flakes based on our classical understanding of a critical nucleus size. This is unlikely based on our previous studies, which suggest that the intercalation-induced phase change is initiated at the topmost or bottom most layer,[15] and these phase transitions occur in a layer-by-layer fashion in 2D materials;[27-29] thus nucleation of the T_d' phase should be insensitive to flake thickness. The third possibility to explain the suppressed phase transition is bending induced in-plane strain due to the c-axis lattice expansion, which might introduce an additional energy barrier to the phase transition. This is what we previously observed in delayed lithium staging in thin graphite flakes.[30] For the phase transition in WTe_2, we observe c-axis lattice expansion of more than 5% (Figure 2). However, we do not observe any shifts of Raman peaks in T_d-WTe_2 during intercalation (Figure S3), which would indicate in-plane tensile strain.[31]

Interpreting peak shifts in Raman spectra for WTe_2 is complicated by the fact that electron doping and tensile strain, both of which lithium intercalation imparts to WTe_2, would result in the opposite shifts in Raman peaks.[32] Nevertheless, the bending-induced strain is unlikely the cause for our observation because the bending-induced strain would increase with increasing thickness, further delaying the phase transition for thicker flakes, which we do not observe.

Finally, we turn our attention to the interface interaction between the SiO_2/Si substrate and the T_d-WTe_2 flake during the phase transition. Compared to the T_d-WTe_2 phase, lithiated T_d'-WTe_2 exhibits an in-plane lattice expansion of 5.2% and 0.2% along the a- and b- axes, respectively, concurrent with a rearrangement of telluride atoms.[22] This significant change of structure induces in-plane strain, which leads to the formation of wrinkled microstructures in WTe_2 flakes supported on the SiO_2/Si substrate (Figure S1 and S2). This in-plane strain is distinct from the bending-induced strain due to the lattice expansion along c- axis discussed previously. Our hypothesis is that the interface between the T_d-WTe_2 flake and the SiO_2/Si substrate anchors the nanoflake, preventing the release of the in-plane strain introduced during the T_d to T_d' phase transition, thus increasing the energy barrier of the phase change. The interfacial effect is likely to affect the bottom-most layer of the T_d-WTe_2 flake that directly contacts the SiO_2/Si substrate. In this case, the substrate effect becomes more pronounced in atomically thin layered samples compared to thicker samples.

Effects of Substrate Interfaces on Phase Transition Kinetics

To test our hypothesis of the interface effect due to the interaction between the substrate and WTe_2, we place our WTe_2 flakes on hBN to weaken the interactions at this heterointerface. An atomic force microscopy (AFM) study has shown that coupling between SiO_2 and Bi_2Se_3 layer is

stronger than that between Bi_2Se_3 layers,[33] supporting our rationale of using hBN. Figure 4 shows a thick T_d-WTe_2 flake (>100 nm) that was partially placed on top of a hBN flake and partially on the SiO_2/Si substrate. This heterostructure was then assembled into a liquid intercalation cell with the Cr/Au electrode contacting both T_d-WTe_2 and hBN. At an V_{EC} of 1.2 V, dark streaks that represent wrinkles and thus the phase transition appeared first at the edge of the hBN supported region after 3 minutes, then in the entire hBN supported region after 6 minutes (Figure 4a). By contrast, it took 14 minutes for the wrinkles to appear in the solely SiO_2/Si supported region. This observation supports the hypothesis that the weak interfacial coupling between T_d-WTe_2 and hBN facilitated the release of in-plain strain introduced by T_d to T_d' phase transition during lithium intercalation, in comparison to the interface between T_d-WTe_2 and the SiO_2/Si substrate.

The rapid phase transition, due to the high ionic conductivity of the liquid electrolyte, made it challenging to acquire the Raman spectra during intercalation. Therefore, we fabricated a polymer cell featuring a 5-layered T_d-WTe_2 flake, half supported on a hBN flake and the other half directly on the SiO_2/Si substrate (Figure 4b). Raman spectra collected during lithium intercalation of this cell are presented in Figure S4, which shows that the T_d to T_d' phase transition occurred at 0.3 V for the SiO_2-supported T_d-WTe_2 region, consistent with the suppressed phase transition discussed earlier. For the hBN supported T_d-WTe_2 region, the Raman spectra changed at 0.4 V, confirming our hypothesis that anchoring to the SiO_2/Si substrate results in the delay of phase transition in thin T_d-WTe_2 nanoflakes.

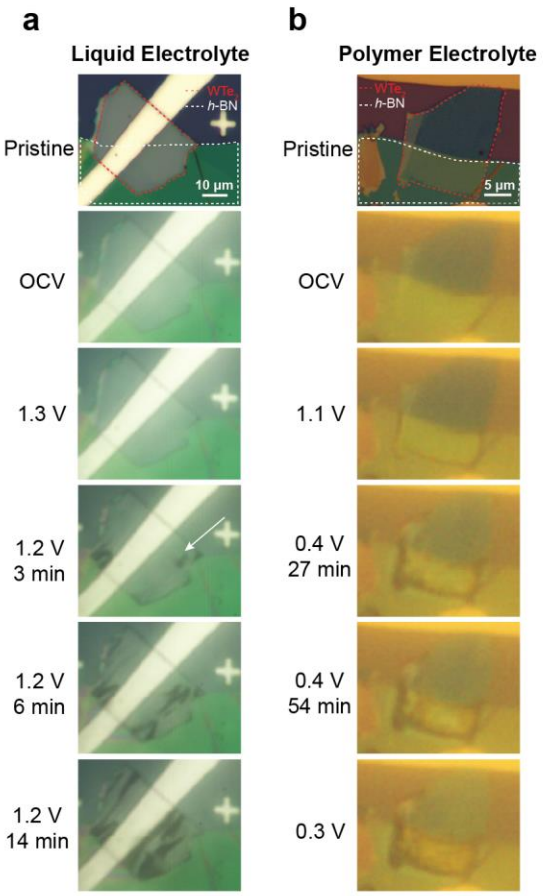

Figure 4. Comparison of phase transition kinetics in T_d-WTe_2 with different substrate interfaces. (a) Optical images of a T_d-WTe_2 nanoflake (red dashed outline) partially supported on a hBN flake (white dashed outline) during lithium intercalation using liquid electrolyte; scale bar, 10 μm. The appearance of dark streaks marks the onset of the phase transition from T_d to lithiated T_d'. (b) Optical images of a T_d-WTe_2 nanoflake (red dashed outline) partially supported on a hBN flake (white dashed outline) collected during lithium intercalation using polymer electrolyte; scale bar, 5 μm. The Raman spectra for (b) are shown in Supplementary Figure S4.

CONCLUSION

In summary, our study showed that the T_d to lithiated T_d' phase transition of WTe_2 flakes is thickness dependent with more applied electrochemical voltage needed for thinner flakes, going from an intercalation voltage of 0.8 V for thicker flakes to 0.5 V for a 7-layered flake to 0. 3 V for a 5-layered flake to trigger the phase transition using a polymer electrolyte. We attribute our observation to strong interactions between WTe_2 and the SiO_2/Si substrate, which hinder effective release of the in-plane strain in WTe_2 during the phase transition. This interfacial interaction becomes more prominent as the thickness of the flake decreases. The observed suppression of the phase transition can be mitigated by proper interface engineering, such as replacing the SiO_2/Si substrate with an hBN flake. Our observations highlight the unique interface interactions of WTe_2, particularly in thinner nanoflakes, during the lithium intercalation process. Such heterointerface effects hold implications for various device applications reliant on phase changes, as they can alter the phase transition dynamics.

EXPERIMENTAL METHODS

Device Fabrication

T_d-WTe_2 and hBN nanoflakes were obtained via mechanical exfoliation from WTe_2 (2D Semiconductors) and hBN (HQ Graphene) bulk by scotch-tape onto SiO_2/Si substrates. Subsequently, a potassium hydroxide (KOH)-assisted transfer method was employed to transfer desired size and thickness-controlled T_d-WTe_2 nanoflakes onto dry thermal oxide SiO_2/Si substrates with alignment marks for lithography.[14] To fabricate the T_d-WTe_2 (top) - hBN (bottom) device, an hBN nanoflake was initially transferred by the same method and then stacked with a WTe_2 nanoflake that sat partially on the hBN nanoflake and partially on the dry thermal oxide SiO_2/Si substrate. The thickness of the T_d-WTe_2 nanoflakes, ranging from 15 layers to bulk, was

determined by a Cypher ES atomic force microscope (AFM) from Asylum Research and a Veeco Dimension Icon AFM. As thin WTe_2 nanoflakes are more likely to oxide compared to thick WTe_2 nanoflakes, the ascertainment of thickness of WTe_2 nanoflakes with 2-15 layers was not conducted by AFM in air; instead, Raman spectroscopy was employed before the intercalation experiment, where thin WTe_2 nanoflakes were protected by an air-tight case from air. The calibration combined Raman spectroscopy and AFM on a standard T_d-WTe_2 sample is showed in Figure S5.

Both e-beam lithography and photolithography were used for device fabrication. For e-beam lithography, electrodes were patterned using Nabity NPGS (installed on a Helios G4 FIB-SEM) and deposited with 10 nm Cr / 100 nm Au using thermal evaporation (MBraun EcoVap). E-beam lithography was used to fabricate devices of WTe_2 (thick and 7-layer flakes) and WTe_2 (top) - hBN (bottom) heterostructures (using liquid electrolyte), as well as thick T_d-WTe_2 flakes for single-crystal XRD experiments. For some devices, electrodes were written using photon lithography (Heidelberg Mask Writer - DWL66FS) and deposited with 10 nm Cr /100 nm Au using an e-beam evaporator (CVC SC4500 Combination Thermal/E-gun Evaporation System). Devices of 5-layered T_d-WTe_2 and T_d-WTe_2 (top) - hBN (bottom) heterostructures for the polymer cell were fabricated this way. All fabricated devices were stored in an argon glovebox to minimize oxidation.

Fabrication of Electrochemical Intercalation Cells

All electrochemical intercalation cells adopted the same planar cell configuration with a T_d-WTe_2 nanoflake or T_d-WTe_2 (top) - hBN (bottom) heterostructure as working electrode and a small piece of lithium metal (~3 by 3 cm, 0.38 mm-thick ribbon, Sigma-Aldrich) as counter/reference electrode. The cell fabrication steps are described in detail in our previous papers.[14-15] The entire cell was encapsulated in a transparent case, with a coverslip serving as the top cover, allowing the laser to interact with the nanoflake during Raman spectroscopy. For liquid intercalation cells, 1 M

lithium hexafluorophosphate ($LiPF_6$ in 50/50 v/v EC/DEC, battery-grade, Sigma Aldrich) was injected into the transparent case as the electrolyte. For the polymer electrolyte cells, 227 mg 1 M $LiPF_6$, 475 mg polymer (poly(ethylene glycol)methyl ether methacrylate (PEGMA, Sigma Aldrich) and 1145 mg Bisphenol A ethoxylate (15EO/phenol) dimethacrylate (BEMA, Sigma Aldrich) were pre-mixed for 4 hours. Following this, 46 mg of 2-Hydroxy-2-methylpropiophenone (photo-initiator, Sigma Aldrich) were added to the blend and stirred for another half hour in the dark prior to use. The mixed polymer was carefully filled into the transparent case of the intercalation cell by a micro-pipette and subsequently cured by exposure to ultraviolet light (UV light, 375 nm, 4 W) for 10 minutes to form a solid polymer electrolyte. All assembly procedures for the electrochemical intercalation cell were conducted inside the glovebox with O_2 and H_2O levels below 0.5 ppm. With the protection provided by the transparent case, the intercalation cell can withstand exposure to air and moisture in the atmosphere for a minimum of 10 hours, making it suitable for subsequent *in-situ* characterization.

***In-situ* Raman Characterization**

Lithium intercalation of the assembled electrochemical intercalation cell was carried out potentiostatically by applying a voltage between the working (T_d-WTe_2 or T_d-WTe_2 - hBN) and counter/reference (Li) electrodes with a Biological SP300 potentiostat/galvanostat. *In-situ* Raman spectra were collected during lithium intercalation, and two types of Raman spectrometers were employed. For the cells of T_d-WTe_2 (thick and 7-layers) and T_d-WTe_2 (top) - hBN (bottom) heterostructure (using liquid electrolyte), a Horiba LabRAM HR Evolution Spectrometer (grating: 1800 lines/mm) with an excitation wavelength of 633 nm at 10% power (~3.5 mW) was used. For the cells of 5-layered T_d-WTe_2 and T_d-WTe_2 (top) - hBN (bottom) heterostructure in the polymer

cell, a WITec Alpha300R Confocal Raman Microscope (grating: 1800 lines/mm) with a laser wavelength of 532 nm and power ranging from 1 to 3 mW was employed.

Prior to intercalation, a Raman spectrum was acquired at the open circuit voltage (OCV), typically ranging between 2.3 to 2.8 V vs. Li^+/Li for T_d-WTe_2 intercalation cells. During the electrochemical intercalation, the voltage applied between the T_d-WTe_2 nanoflake and the lithium electrode (V_{EC}) was lowered at a controlled rate of 10 mV/s, and then maintained at the desired voltage until multiple Raman spectra were collected. Simultaneously, optical images were captured using the camera of the Raman microscope and the contrast of those images was changed to clearly observe the wrinkle formation during intercalation. The observed differences in contrast and brightness between the pristine T_d-WTe_2 and other optical images during intercalation are attributed to the presence of the electrolyte and coverslip.

***In-situ* Single-Crystal XRD Characterization**

The single-crystal X-ray diffraction (XRD) experiments were carried out at beamline 4-ID Integrated *In situ* and Resonant Hard X-ray Studies (ISR) of National Synchrotron Light Source II at Brookhaven National Laboratory, using a beam energy of 11.5 keV and a spot size of 300 μm by 300 μm. The configuration of the electrochemical intercalation cells for the single-crystal XRD differs slightly from that in the Raman spectroscopy study. An ample amount of polymer electrolyte was carefully applied on the device, covering both the T_d-WTe_2 device and Li, and then cured by UV light for 10 minutes without the transparent cover slip. This cured polymer electrolyte provided sufficient protection for the T_d-WTe_2 device and Li against air and moisture for at least 3 hours, allowing the intercalation experiments to be completed within 2 hours. However, prolonged X-ray exposure gradually deteriorated the polymer electrolyte, leading to disconnection of the intercalation cell circuit. The lithiated T_d' phase reverted to the T_d phase immediately after

the cell circuit was disconnected. To mitigate this issue, the X-ray beam exposure was kept to a minimum, and solely focused on collecting data related to the Bragg reflection change in the reciprocal lattice of the (002) plane.

Post-intercalation SEM Characterization

After electrochemical intercalation, the cells were dissembled, and the electrolyte was carefully removed. Then, the T_d-WTe_2 devices were washed with isopropyl alcohol, dried, and characterized by a scanning electron microscope (HeliosG4 FIB-SEM or Tescan Mira3 FESEM) at various tilt angles of 0°, 45° and 50°.

ASSOCIATED CONTENT

The Supporting Information is available free of charge at

Supporting figures (S1—S5) (PDF)

AUTHOR INFORMATION

Corresponding Author

Judy J. Cha – Department of Materials Science and Engineering, Cornell University, Ithaca, New York, 14853, United States; Email: jc476@cornell.edu

Authors

Shiyu Xu – Department of Mechanical Engineering and Materials Science, Yale University, New Haven, Connecticut, 06511, United States; Department of Materials Science and Engineering, Cornell University, Ithaca, New York, 14853, United States

Mengjing Wang – Department of Materials Science and Engineering, Cornell University, Ithaca, New York, 14853, United States

Maria Bambrick-Santoyo – Department of Applied Physics, Yale University, New Haven, Connecticut, 06511, United States

Kenneth Evans-Lutterodt –National Synchrotron Light Source II, Brookhaven National Laboratory, Upton, New York, 11973, United States

Natalie L. Williams – Department of Chemistry and Chemical Biology, Cornell University, Ithaca, New York, 14853, United States

Judy J. Cha – Department of Materials Science and Engineering, Cornell University, Ithaca, New York, 14853, United States

Author Contributions

S.X. and M.W. contributed equally. S.X. and M.W. carried out the experiments and analyzed the data. M.B.S. helped carry out experiments for the WTe_2-hBN heterostructures. K.E. conducted the single-crystal XRD experiments. S.X., M.W., N.L.W. and J.J.C. wrote the manuscript with input from all authors. All authors have given approval to the final version of the manuscript.

Notes

The authors declare no competing financial interest.

ACKNOWLEDGMENT

S.X., M.W. and J.J.C. gratefully acknowledge support from the Gordon and Betty Moore Foundation's EPiQS Initiative, grant GBMF9062.01 and National Science Foundation (CBET

#2240944). Device fabrication and characterization for some devices were carried out at the Yale West Campus Materials Characterization Core and the Yale West Campus Cleanroom. This work was performed in part at the Cornell NanoScale Facility, a member of the National Nanotechnology Coordinated Infrastructure (NNCI), which is supported by the National Science Foundation (Grant NNCI-2025233). The authors acknowledge the use of facilities and instrumentation supported by NSF through the Cornell University Materials Research Science and Engineering Center DMR-1719875. This research used beamline 4-ID of the National Synchrotron Light Source II, a U.S. Department of Energy (DOE) Office of Science User Facility operated for the DOE Office of Science by Brookhaven National Laboratory under Contract No. DE-SC0012704.

REFERENCES

(1) Zeng, M.; Xiao, Y.; Liu, J.; Yang, K.; Fu, L. Exploring Two-Dimensional Materials toward the Next-Generation Circuits: From Monomer Design to Assembly Control. *Chemical Reviews* **2018,** *118* (13), 6236-6296, DOI: 10.1021/acs.chemrev.7b00633.
(2) Voiry, D.; Yamaguchi, H.; Li, J.; Silva, R.; Alves, D. C.; Fujita, T.; Chen, M.; Asefa, T.; Shenoy, V. B.; Eda, G.; Chhowalla, M. Enhanced catalytic activity in strained chemically exfoliated WS_2 nanosheets for hydrogen evolution. *Nat Mater* **2013,** *12* (9), 850-5, DOI: 10.1038/nmat3700.
(3) Iannaccone, G.; Bonaccorso, F.; Colombo, L.; Fiori, G. Quantum engineering of transistors based on 2D materials heterostructures. *Nat Nanotechnol* **2018,** *13* (3), 183-191, DOI: 10.1038/s41565-018-0082-6.
(4) Wang, Q. H.; Kalantar-Zadeh, K.; Kis, A.; Coleman, J. N.; Strano, M. S. Electronics and optoelectronics of two-dimensional transition metal dichalcogenides. *Nat Nanotechnol* **2012,** *7* (11), 699-712, DOI: 10.1038/nnano.2012.193.
(5) Liu, J.; Cao, H.; Jiang, B.; Xue, Y.; Fu, L. Newborn 2D materials for flexible energy conversion and storage. *Science China Materials* **2016,** *59* (6), 459-474, DOI: 10.1007/s40843-016-5055-5.
(6) Wang, Y.; Xiao, J.; Zhu, H.; Li, Y.; Alsaid, Y.; Fong, K. Y.; Zhou, Y.; Wang, S.; Shi, W.; Wang, Y.; Zettl, A.; Reed, E. J.; Zhang, X. Structural phase transition in monolayer MoTe(2) driven by electrostatic doping. *Nature* **2017,** *550* (7677), 487-491, DOI: 10.1038/nature24043.
(7) Song, S.; Keum, D. H.; Cho, S.; Perello, D.; Kim, Y.; Lee, Y. H. Room Temperature Semiconductor-Metal Transition of MoTe2 Thin Films Engineered by Strain. *Nano Lett* **2016,** *16* (1), 188-93, DOI: 10.1021/acs.nanolett.5b03481.
(8) Xiong, F.; Wang, H.; Liu, X.; Sun, J.; Brongersma, M.; Pop, E.; Cui, Y. Li Intercalation in MoS2: In Situ Observation of Its Dynamics and Tuning Optical and Electrical Properties. *Nano Letters* **2015,** *15* (10), 6777-6784, DOI: 10.1021/acs.nanolett.5b02619.

(9) Wang, M.; Xu, S.; Cha, J. J. Revisiting Intercalation-Induced Phase Transitions in 2D Group VI Transition Metal Dichalcogenides. *Advanced Energy and Sustainability Research* **2021,** *2* (8), 2100027, DOI: https://doi.org/10.1002/aesr.202100027.
(10) Keum, D. H.; Cho, S.; Kim, J. H.; Choe, D.-H.; Sung, H.-J.; Kan, M.; Kang, H.; Hwang, J.-Y.; Kim, S. W.; Yang, H.; Chang, K. J.; Lee, Y. H. Bandgap opening in few-layered monoclinic MoTe2. *Nat Phys* **2015,** *11* (6), 482-486, DOI: 10.1038/nphys3314.
(11) Cho, S.; Kim, S.; Kim, J. H.; Zhao, J.; Seok, J.; Keum, D. H.; Baik, J.; Choe, D.-H.; Chang, K. J.; Suenaga, K.; Kim, S. W.; Lee, Y. H.; Yang, H. Phase patterning for ohmic homojunction contact in MoTe2. *Science* **2015,** *349* (6248), 625-628, DOI: 10.1126/science.aab3175.
(12) Ahmed, S.; Yi, J. Two-Dimensional Transition Metal Dichalcogenides and Their Charge Carrier Mobilities in Field-Effect Transistors. *Nano-Micro Letters* **2017,** *9* (4), 50, DOI: 10.1007/s40820-017-0152-6.
(13) Radisavljevic, B.; Radenovic, A.; Brivio, J.; Giacometti, V.; Kis, A. Single-layer MoS2 transistors. *Nature Nanotechnology* **2011,** *6* (3), 147-150, DOI: 10.1038/nnano.2010.279.
(14) Yazdani, S.; Pondick, J. V.; Kumar, A.; Yarali, M.; Woods, J. M.; Hynek, D. J.; Qiu, D. Y.; Cha, J. J. Heterointerface Effects on Lithium-Induced Phase Transitions in Intercalated MoS2. *ACS Applied Materials & Interfaces* **2021,** *13* (8), 10603-10611, DOI: 10.1021/acsami.0c21495.
(15) Pondick, J. V.; Kumar, A.; Wang, M.; Yazdani, S.; Woods, J. M.; Qiu, D. Y.; Cha, J. J. Heterointerface Control over Lithium-Induced Phase Transitions in MoS2 Nanosheets: Implications for Nanoscaled Energy Materials. *ACS Applied Nano Materials* **2021,** *4* (12), 14105-14114, DOI: 10.1021/acsanm.1c03402.
(16) Pondick, J. V.; Yazdani, S.; Kumar, A.; Hynek, D. J.; Hart, J. L.; Wang, M.; Qiu, D. Y.; Cha, J. J. Thickness-dependent phase transition kinetics in lithium-intercalated MoS2. *2D Materials* **2022,** *9* (2), 025009, DOI: 10.1088/2053-1583/ac4e9b.
(17) Fei, Z.; Palomaki, T.; Wu, S.; Zhao, W.; Cai, X.; Sun, B.; Nguyen, P.; Finney, J.; Xu, X.; Cobden, D. H. Edge conduction in monolayer WTe2. *Nat Phys* **2017,** *13* (7), 677-682, DOI: 10.1038/nphys4091.
(18) Fatemi, V.; Wu, S.; Cao, Y.; Bretheau, L.; Gibson, Q. D.; Watanabe, K.; Taniguchi, T.; Cava, R. J.; Jarillo-Herrero, P. Electrically tunable low-density superconductivity in a monolayer topological insulator. *Science* **2018,** *362* (6417), 926-929, DOI: 10.1126/science.aar4642.
(19) Sajadi, E.; Palomaki, T.; Fei, Z.; Zhao, W.; Bement, P.; Olsen, C.; Luescher, S.; Xu, X.; Folk, J. A.; Cobden, D. H. Gate-induced superconductivity in a monolayer topological insulator. *Science* **2018,** *362* (6417), 922-925, DOI: 10.1126/science.aar4426.
(20) Zhu, L.; Li, Q. Y.; Lv, Y. Y.; Li, S.; Zhu, X. Y.; Jia, Z. Y.; Chen, Y. B.; Wen, J.; Li, S. C. Superconductivity in Potassium-Intercalated T (d)-WTe(2). *Nano Lett* **2018,** *18* (10), 6585-6590, DOI: 10.1021/acs.nanolett.8b03180.
(21) Fei, Z.; Zhao, W.; Palomaki, T. A.; Sun, B.; Miller, M. K.; Zhao, Z.; Yan, J.; Xu, X.; Cobden, D. H. Ferroelectric switching of a two-dimensional metal. *Nature* **2018,** *560* (7718), 336-339, DOI: 10.1038/s41586-018-0336-3.
(22) Muscher, P. K.; Rehn, D. A.; Sood, A.; Lim, K.; Luo, D.; Shen, X.; Zajac, M.; Lu, F.; Mehta, A.; Li, Y.; Wang, X.; Reed, E. J.; Chueh, W. C.; Lindenberg, A. M. Highly Efficient Uniaxial In-Plane Stretching of a 2D Material via Ion Insertion. *Advanced Materials* **2021,** *33* (37), 2101875, DOI: https://doi.org/10.1002/adma.202101875.
(23) Wang, M.; Kumar, A.; Dong, H.; Woods, J. M.; Pondick, J. V.; Xu, S.; Hynek, D. J.; Guo, P.; Qiu, D. Y.; Cha, J. J. A Gapped Phase in Semimetallic Td-WTe2 Induced by Lithium Intercalation. *Advanced Materials* **2022,** *34* (24), 2200861, DOI: https://doi.org/10.1002/adma.202200861.

(24) Zhou, Y.; Silva, J. L.; Woods, J. M.; Pondick, J. V.; Feng, Q.; Liang, Z.; Liu, W.; Lin, L.; Deng, B.; Brena, B.; Xia, F.; Peng, H.; Liu, Z.; Wang, H.; Araujo, C. M.; Cha, J. J. Revealing the Contribution of Individual Factors to Hydrogen Evolution Reaction Catalytic Activity. *Advanced Materials* **2018,** *30* (18), 1706076, DOI: https://doi.org/10.1002/adma.201706076.
(25) Nair, J. R.; Gerbaldi, C.; Destro, M.; Bongiovanni, R.; Penazzi, N. Methacrylic-based solid polymer electrolyte membranes for lithium-based batteries by a rapid UV-curing process. *Reactive and Functional Polymers* **2011,** *71* (4), 409-416, DOI: https://doi.org/10.1016/j.reactfunctpolym.2010.12.007.
(26) Xiang, F.-X.; Srinivasan, A.; Du, Z. Z.; Klochan, O.; Dou, S.-X.; Hamilton, A. R.; Wang, X.-L. Thickness-dependent electronic structure in WTe2 thin films. *Physical Review B* **2018,** *98* (3), 035115, DOI: 10.1103/PhysRevB.98.035115.
(27) Lee, C.-H.; Ryu, H.; Nolan, G.; Zhang, Y.; Lee, Y.; Oh, S.; Cheong, H.; Watanabe, K.; Taniguchi, T.; Kim, K.; Lee, G.-H.; Huang, P. Y. In Situ Imaging of an Anisotropic Layer-by-Layer Phase Transition in Few-Layer MoTe2. *Nano Letters* **2023,** *23* (2), 677-684, DOI: 10.1021/acs.nanolett.2c04550.
(28) Parida, S.; Mishra, A.; Chen, J.; Wang, J.; Dobley, A.; Carter, C. B.; Dongare, A. M. Vertically Stacked 2H-1T Dual-Phase MoS2 Microstructures during Lithium Intercalation: A First Principles Study. *Journal of the American Ceramic Society* **2020,** *103* (11), 6603-6614, DOI: https://doi.org/10.1111/jace.17367.
(29) Sung, S. H.; Schnitzer, N.; Novakov, S.; El Baggari, I.; Luo, X.; Gim, J.; Vu, N. M.; Li, Z.; Brintlinger, T. H.; Liu, Y.; Lu, W.; Sun, Y.; Deotare, P. B.; Sun, K.; Zhao, L.; Kourkoutis, L. F.; Heron, J. T.; Hovden, R. Two-dimensional charge order stabilized in clean polytype heterostructures. *Nature Communications* **2022,** *13* (1), 413, DOI: 10.1038/s41467-021-27947-5.
(30) Pondick, J. V.; Yazdani, S.; Yarali, M.; Reed, S. N.; Hynek, D. J.; Cha, J. J. The Effect of Mechanical Strain on Lithium Staging in Graphene. *Advanced Electronic Materials* **2021,** *7* (3), 2000981, DOI: https://doi.org/10.1002/aelm.202000981.
(31) Yang, W.; Yuan, Z.-Y.; Luo, Y.-Q.; Yang, Y.; Zheng, F.-W.; Hu, Z.-H.; Wang, X.-H.; Liu, Y.-A.; Zhang, P. Raman-active modes of 1T' — WTe2 under tensile strain: A first-principles prediction. *Physical Review B* **2019,** *99* (23), 235401, DOI: 10.1103/PhysRevB.99.235401.
(32) Yang, W.; Fu, S.-B.; Lu, Y.; Zhang, K.-Y.; Liu, J.-M.; Gao, H.-R.; Wang, X.-H.; Liu, Y.-A.; Zhang, P. Response of Raman-active modes in monolayer 1T'-WTe2 to charge doping. *Physical Review B* **2022,** *106* (20), 205415, DOI: 10.1103/PhysRevB.106.205415.
(33) Hong, S. S.; Kundhikanjana, W.; Cha, J. J.; Lai, K.; Kong, D.; Meister, S.; Kelly, M. A.; Shen, Z.-X.; Cui, Y. Ultrathin Topological Insulator Bi2Se3 Nanoribbons Exfoliated by Atomic Force Microscopy. *Nano Letters* **2010,** *10* (8), 3118-3122, DOI: 10.1021/nl101884h.